Hindawi
Geofluids
Volume 2020, Article ID 8849444, 12 pages
https://doi.org/10.1155/2020/8849444

Research Article

Research on the Pore Evolution of Sandstone in Cold Regions under Freeze-Thaw Weathering Cycles Based on NMR

Zheng Pan,[1,2] **Keping Zhou**,[1,2] **Rugao Gao**,[1,2,3] **Zhen Jiang**,[1,2] **Chun Yang**,[1,2] **and Feng Gao**[1,2]

[1]*School of Resources and Safety Engineering, Central South University, Changsha, 410083 Hunan, China*
[2]*Research Center for Mining Engineering and Technology in Cold Regions, Central South University, Changsha, 410083 Hunan, China*
[3]*Department of Mining and Materials Engineering, McGill University 3450 Rue University Montreal, QC, Canada H3A 2A7*

Correspondence should be addressed to Rugao Gao; gaorgcsu@csu.edu.cn

Received 29 September 2020; Revised 19 October 2020; Accepted 24 October 2020; Published 20 November 2020

Academic Editor: Chun Zhu

The evolution of the rock pore structure is an important factor influencing rock mechanical properties in cold regions. To study the mesoscopic evolution law of the rock pore structure under freeze-thaw weathering cycles, a freeze-thaw weathering cycle experiment was performed on red sandstone from the cold region of western China with temperatures ranging from -20°C to +20°C. The porosity, T2 spectral distribution, and magnetic resonance imaging (MRI) characteristics of the red sandstone after 0, 20, 40, 60, 80, 100, and 120 freeze-thaw weathering cycles were measured by the nondestructive detection technique nuclear magnetic resonance (NMR). The results show that the porosity of sandstone decreases first and then increases with the increase of the freeze-thaw weathering cycles and reaches the minimum at 60 of freeze-thaw weathering cycles. The evolution characteristics of porosity can be divided into three stages, namely, the abrupt decrease in porosity, the slow decrease in porosity, and the steady increase in porosity. The evolution characteristics of the T2 spectrum distribution, movable fluid porosity (MFP), and MRI images in response to the freeze-thaw weathering process are positively correlated with the porosity. Analysis of the experimental data reveals that the decrease in the porosity of the red sandstone is mainly governed by mesopores, which is related to the water swelling phenomenon of montmorillonite. Hence, the pore connectivity decreases. As the number of freeze-thaw cycles increases, the effect of the hydrophysical reaction on the porosity gradually disappears, and the frost heaving effect caused by the water-ice phase transition gradually dominates the pore evolution law of red sandstone.

1. Introduction

Rock is a natural three-phase porous dielectric material formed during a long geological process, and numerous micropores, microcracks, and microdefects are contained within [1–3]. In cold regions, the ever-changing climate makes these natural microdefects of the rock mass vulnerable to freeze-thaw weathering cycles and causes fatigue damage, which changes the physical and mechanical properties of the rock mass and imposes an important impact on rock engineering [4–6]. When the temperature is lower than 0°C, a certain volume of liquid water inside the rock freezes, which will increase by approximately 9%, and a frost heaving force is generated on the sidewalls of pores so that they expand. With increasing temperature, the ice melts, and the pores are replenished with liquid water [7]. Cold regions occupy a large part of the human living environment. Currently, many geotechnical projects are deeply affected by freeze-thaw weathering disasters. Therefore, the experimental study of the evolution of the rock microstructure under the conditions of freeze-thaw weathering cycles has an important practical significance to reveal the mechanism of rock damage and guarantee rock engineering in cold regions.

Methods such as computed tomography (CT) [8–10], scanning electron microscopy (SEM) [11], nuclear magnetic resonance (NMR) [12–14], microseismic monitoring (MS)

[15], and acoustic emission (AE) [16] have been adopted in previous studies to clarify the relationship between pore structure degradation and rock mechanical properties under freeze-thaw cycles and to protect rock mechanical engineering. There are more and more reports on the use of NMR technology to detect rock damage. For example, Liu [17, 18] studied the internal microstructure changes in rock under the influence of the freeze-thaw treatment by the NMR technique. He found that rock microstructure deteriorated under the influence of freeze-thaw cycles. With the increase of freeze-thaw cycles, the volume of macropores in the rock increased, while the volume of micropores showed fluctuations. Hu [19, 20] obtained the T2 spectra of the grouting materials by NMR technique, which reflected the evolutionary relationship of the five microstructure of interlayer pores, gel pores, capillary pores, circular air holes, and fractures with curing time. He also used NMR, SEM, and fractal theory to establish the quantitative relationship of microscopic characterization between the action of air-entraining agents and cemented paste backfill pore structure. Zhai [21] implemented NMR and SEM to analyze the pore distribution characteristics of coal samples and found that the freeze-thaw effect causes the development, penetration, and expansion of the pores in the coal samples. Jia [22] applied NMR technology to study the freezing process of sandstone pore water and divided the whole process into four stages: supercooling, rapid freezing, stable freezing, and freezing cessation. The T2 spectrum distribution of rock is obtained through NMR testing, including the pore information and pore size distribution characteristics of the rock after freeze-thaw weathering cycles [23]. The changes in the pore structure reflect the degradation characteristics of the microstructure after the rock undergoes freeze-thaw weathering cycles. When the frost heaving force is greater than the binding force between mineral particles, the porosity increases sharply [13, 14]. Wang [24] used NMR and AE techniques to study the failure mechanism of rocks under cyclic mechanical loads and freeze-thaw weathering cycles. Their results showed that the pores in rocks subjected to freeze-thaw degradation deteriorated faster, and the strength of rocks subjected to the combined treatment of cyclic loads and freeze-thaw cycles was reduced by approximately 30%.

Under the freeze-thaw weathering cycle effect, the change in rock mechanical properties is caused by the deterioration of the internal pore structure. Therefore, many researchers [25–30] have conducted much research through indoor experiments, numerical simulations, damage models, etc. Jiang [31] studied the response mechanism of two kinds of marble microstructures to the dynamic cyclic impact under the condition of freeze-thaw weathering cycles, and he found that under the cyclic dynamic impact, the two marble types exhibited the same trend: the porosity gradually decreased, the pore size continuously decreased, the pore structure tightened, and the permeability weakened. Weng [32] et al. studied the response mechanism of the rock microstructure and dynamic mechanical behaviour to freeze-thaw weathering cycles. Martins [33] studied the influence of freeze-thaw weathering cycles on the physical and mechanical properties of granite. Huang [34, 35] constructed a constitutive model of rock damage under freeze-thaw and load conditions, as well as the thermal-hydraulic-mechanical (THM) coupling control equation of frozen rock under low-temperature conditions, and achieved good prediction results.

Furthermore, the deterioration of the pore structure is an important factor causing rock damage. Therefore, it is particularly important to accurately measure pores under freeze-thaw weathering cycles. The pore measurement methods implemented by researchers include mercury intrusion porosimetry (MIP) [36–38], oven-drying method [39, 40], and NMR [13, 41]. MIP destroys the internal pore structure of the rock and cannot be continuously observed. The oven-drying method heats rock to temperatures above 100°C, which may cause further rock damage. NMR is the only non-destructive testing technique, which implies that no interference damage occurs to the sample, and it can track pore changes and has a certain degree of repeatability. In recent years, NMR technology has been gradually applied for the detection and damage identification of rock mesostructures. It can realize multiscale and multiparameter synchronous recognition, exhibits a high sensitivity to pore fluids, and yields quantitative characteristics.

However, most researchers have focused on the macro-mechanical behaviour of rocks after freeze-thaw weathering cycles, and there are few studies specifically on the evolution of the rock pore structure during freeze-thaw weathering cycles. In this study, a series of freeze-thaw weathering cycle experiments were conducted on red sandstone. The process of freeze-thaw weathering damage of sandstone was measured by NMR technology. The porosity, T2 spectral distribution, permeability, and MRI images of sandstone during freeze-thaw weathering cycles were evaluated and discussed. According to the experimental results, the evolution law and reason for the pore structure and pore connectivity changes in the red sandstone were analyzed and obtained.

2. Experimental Setup and Test Procedures

2.1. Rock Specimen Preparation. The rock samples were processed from the same coarse-grained red sandstone sampled in the cold region of western China, which ensures the uniformity and integrity of the samples to the greatest extent. The rock samples were prepared into standard cylindrical samples with a height of 50 mm and a diameter of 50 mm, with a height-diameter ratio of 1 : 1. X-ray fluorescence spectroscopy (XRF) was performed on the rock samples, and the mineral composition is summarized in Table 1.

Before the experiment, the mass, initial porosity, and P-wave velocity were measured to remove the more discrete samples. The average mass of the remaining samples was 242.98 g, the average density was 2490.82 kg/m^3, and the average porosity was 6.31%.

2.2. Experimental Facilities. As shown in Figure 1, the TDS-300 freeze-thaw device manufactured by the Suzhou Donghua Testing Instrument Co., Ltd., was used to simulate the environmental and temperature changes in the cold region where the rock was sourced from and conduct freeze-thaw weathering cycle experiments on the rock samples.

Table 1: Mineral constituent elements of the red sandstone.

Mineral elements	O	Si	C	Al	Na	Mg	K	Ca	Others
Content/%	65.74	12.14	9.55	4.01	3.20	2.81	0.33	0.54	1.68

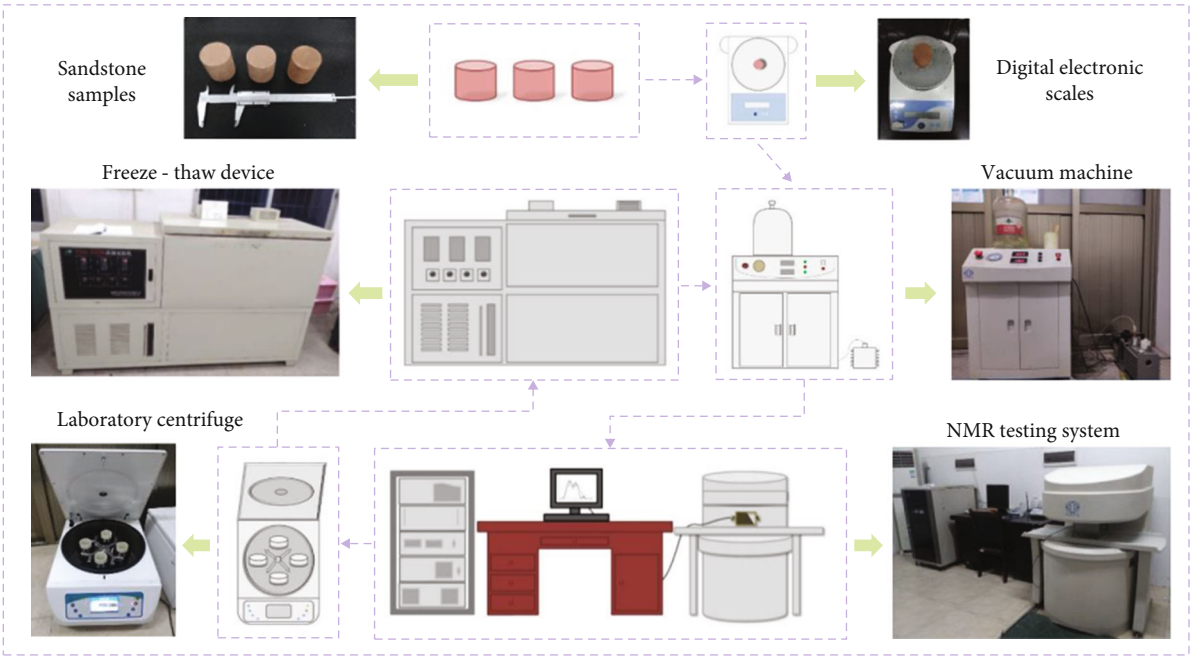

Figure 1: Simple experimental procedure and experimental devices including digital electronic scales, vacuum machine, freeze-thaw device, laboratory centrifuge, and nuclear magnetic resonance test system.

A TDYX-5B low-speed centrifuge was employed for sample centrifugation.

The AnimR-150 rock nuclear magnetic resonance imaging analysis system manufactured by the Suzhou Neumay Electronics Technology Co., Ltd., was adopted to conduct NMR tests on the samples under the conditions of saturation and centrifugation and obtain data including the porosity, T2 spectral distribution, and MRI images of the samples. The magnetic field intensity range was 0.3 T ± 0.05 T.

All experiments were completed in the laboratory of the School of Resources and Safety Engineering and Research Center for Mining Engineering and Technology in Cold Regions, Central South University, China.

2.3. Experimental Procedure. The experimental process is shown in Figure 2. After preparing the samples, the following tests were performed:

(1) *Basic Measurement Test*. The height and diameter of the samples were measured, and the volume of the samples was calculated to provide basic data for the measurement of the porosity

(2) *Freeze-Thaw Cycle Test*. The samples were placed in the TDS-300 freeze-thaw cycle device. According to the climatic conditions of the rock source region, the samples were set to freeze at -20°C for 4 h and were thawed at 20°C for 4 h, i.e., every freeze-thaw weathering cycle lasted 8 h. The NMR measurements were performed every 20 freeze-thaw weathering cycles. The samples were subjected to 0, 20, 40, 60, 80, 100, and 120 freeze-thaw weathering cycles

(3) *NMR Test*. After every 20 freeze-thaw weathering cycles, the samples were taken out and further conditioned in a vacuum saturation device. The samples were dried via drainage for 240 min and saturated for 120 min under a vacuum pressure of 0.1 MPa and then naturally saturated with distilled water for 24 h to ensure that the pores inside the rock samples were filled with water. Then, the saturated rock samples were dried, wrapped with plastic wrap, and tested in the ANIMR-150 type NMR test system to obtain the porosity, T2 spectrum distribution, MRI images, and other information of the samples

(4) *Centrifugation Test*. After the NMR test on the saturated samples was completed, the samples were centrifuged in a TDYX-5B low-speed centrifuge at a speed of 4000 r/min for 60 min. Then, the NMR test was performed again to obtain the micropore information of the samples

(5) Steps (2)–(4) were repeated after completing the NMR tests under saturation and centrifugation

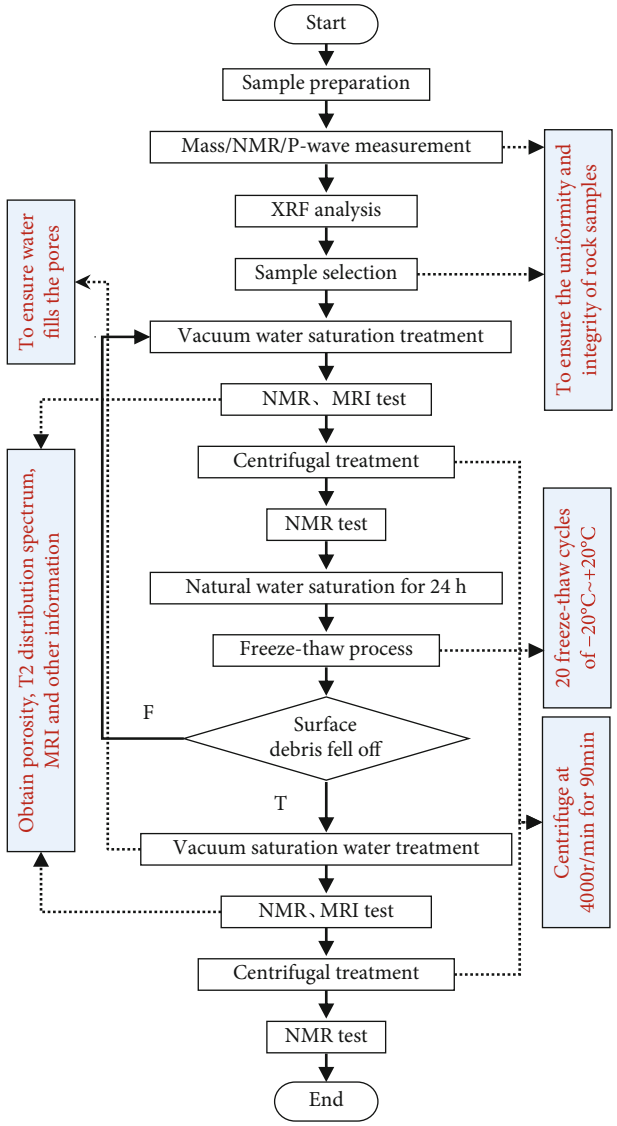

Figure 2: Experimental procedures.

conditions. When debris fell off the sample surface, NMR tests were performed under the final saturation and centrifugation conditions, after which the test was completed

3. Experimental Results and Discussion

3.1. Porosity. The porosity is the ratio of the pore volume to the total rock volume, a macroscopic physical quantity that represents the microscopic structure and reflects the overall state of discontinuous pores in the rock [42]. Therefore, it represents the microscopic rock structure and damage. NMR measures the porosity of saturated rock samples by detecting the nuclear magnetic signal of the pore fluid. The porosity of the samples obtained by NMR after every 20 freeze-thaw weathering cycles is plotted in Figure 3. The porosity of the red sandstone shows an overall trend of first decreasing and then increasing throughout the freeze-thaw

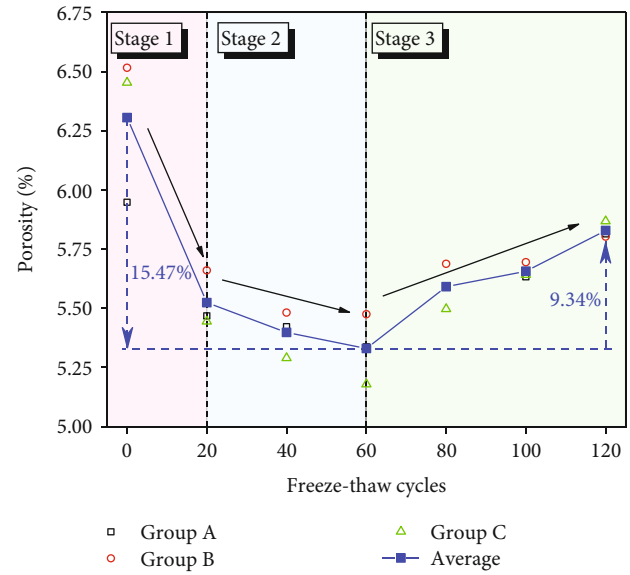

Figure 3: Change in the porosity of the red sandstone with the freeze-thaw weathering cycles.

weathering cycles and reaches a minimum after 60 freeze-thaw weathering cycles.

According to Figure 3, the change in porosity could be described as a three-stage process, namely, the first stage is the abrupt decrease in porosity over 0-20 freeze-thaw weathering cycles, the second stage is the slow decrease in porosity over 20-60 freeze-thaw weathering cycles, and the third stage is the steady increase in porosity over 60-80 freeze-thaw weathering cycles. In the first stage, the average porosity of the samples decreased from 6.306% to 5.524%, 12.4% lower than the initial porosity. In the second stage, the sample porosity decreased further by 0.19%, which is less than that in the first stage. Moreover, the porosity reached its minimum value and decreased by 15.47% over the initial porosity. In the third stage, the porosity gradually increased from 5.331% to 5.828%, an increase of 9.34%.

Under the freezing effect, the pore water inside the rock undergoes a phase change, the frost heaving force generated by the water-ice phase change is applied to the inner walls of the pores to promote their expansion and penetration, and the pore water is replenished after the ice melts [7]. Freeze-thaw weathering cycles commonly increase the rock porosity, but the experimental results reveal that the rock porosity decreases, which indicates that the freeze-thaw weathering process is not the only factor impacting the pore change in this case of red sandstone. The change in porosity is a qualitative characterization of the change in the pore structure, which is caused by the change in the pore number and size. Therefore, to better reveal the evolution characteristics of the pore microstructure in the rock, further quantitative analysis of the T2 spectrum distribution is necessary.

3.2. T2 Spectral Distribution by NMR. In rock NMR measurements, T2 is the time constant describing the recovery process of the ^{1}H proton magnetization transverse component of the pore fluid, which is obtained by inversion of the spin

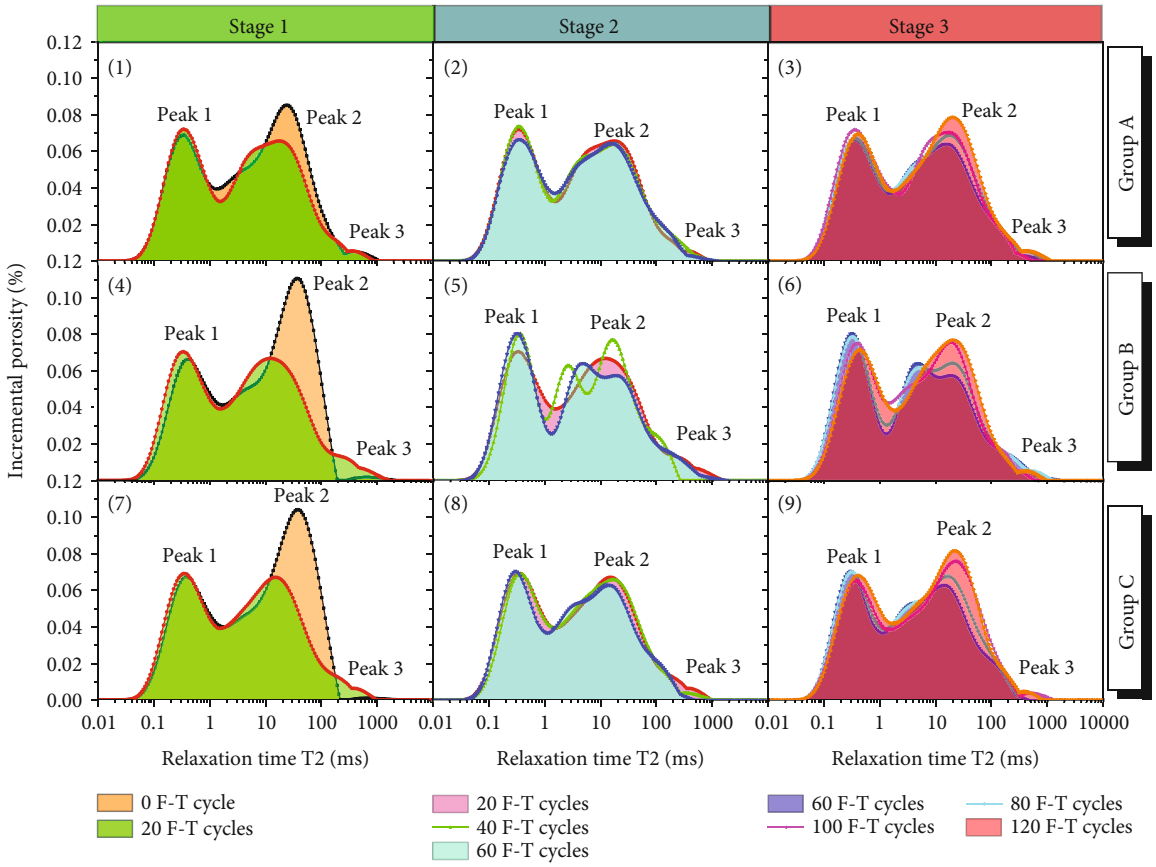

Figure 4: The T2 spectrum distribution evolution of the red sandstone with the freeze-thaw weathering cycles ((1)~(3) for group A, (4)~(6) for group B, and (7)~(9) for group C).

echo series. The T2 spectrum distribution contains information on the pore size and number, and the T2 value is positively correlated with the pore size, while the peak amplitude is positively correlated with the pore number [43]. As the 0 freeze-thaw weather cycle is shown in Figure 4, the T2 spectrum distribution allows a further analysis of the causes of porosity change. The T2 value range of the red sandstone is between 0.01 and 3000 ms, which means that the pore size range is relatively wide. The T2 spectrum contains three peaks, and the amplitude of peaks 1 and 2 is notably higher than that of peak 3, representing three pore types, i.e., small, medium, and large pores, respectively. The T2 spectrum distribution of sandstone is strongly correlated with the change in porosity in response to freeze-thaw weathering cycles. To analyze the relationship between the pore structure evolution and porosity change, the T2 spectrum distribution was divided into three stages according to the porosity change, as shown in Figure 4.

In the first stage, the T2 spectrum changed greatly after 20 freeze-thaw cycles, indicating that the pore structure evolved greatly. Peak 1 moved slightly to the left, and the peak increased slightly. This phenomenon indicates that some small pores are produced at this stage, and the small pores increase slightly. Peak 2 decreased significantly, peak area decreased, indicating that the number of pores decreased sharply. The change in peak 3 was not large, but it exhibited an increasing trend. This indicates that new micropores are generated in the sandstone in response to the freeze-thaw weathering cycles. However, a certain factor inhibits the expansion of the pore size of primary pores by the frost heaving force generated by the water-ice phase transition, which is the most significant for the medium pores represented by peak 2.

In the second stage, the amplitude of peak 1 increased, while peaks 2 and 3 changed little. This indicates that the second stage is a transitional stage. The inhibition and frost heave in the first stage are mutually exclusive. The pore structure greatly evolved, but the porosity did not change much, and only a few pores were formed.

In the third stage, peaks 1, 2, and 3 all moved to the right and tended to increase. This indicates that freeze-thaw weathering gradually dominated, the number and pore size of all pore types increased, and the internal cracks in the rock expanded, among which the medium pores represented by peak 2 were the most obvious.

There is some effect on the sandstone used in this study that is contrary to the water-ice phase transition during the freeze-thaw weathering process, according to the variation characteristics of the three stages of the T2 spectrum. The effect is obvious in the first stage and has a great influence on the medium pores represented by peak 2. After 60 freeze-thaw weathering cycles, the frost heave caused by

water-ice phase transition plays an important role in the evolution of the pore structure.

3.3. Pore Size. NMR reflects the internal structure of rocks by detecting the nuclear magnetic signals of the pore fluids. When the rock sample is completely saturated and placed in a uniform magnetic field with a short echo time, NMR relaxation occurs mainly at the solid-liquid interface inside the rock, which is approximately equal to the surface relaxation of the pore fluid. The surface relaxation rate is independent of the temperature and pressure and related to the specific surface area (the ratio of the pore surface area to the pore volume) [44], which is expressed as

$$\frac{1}{T_2} \approx \rho_2 \left(\frac{S}{V}\right), \tag{1}$$

where $1/T_2$ is the relaxation rate (ms^{-1}) and ρ_2 is the transverse surface relaxation rate of the rock ($\mu m \bullet ms^{-1}$). It has been found that the value range of ρ_2 in different rocks is notably different, even for similar rocks, and its value is closely related to the mineral composition and content [45]. Shumskayte [46] obtained ρ_2 values for red sandstone between 0.003 and 0.006 m/ms, and $\rho_2 = 0.005\,\mu m/ms$ was selected from the lithology comparison. In addition, S/V is the specific surface area (μm^{-1}).

Assuming that all pores have simple shapes, the relation between the pore radius and pore specific surface area is as follows:

$$\frac{F_S}{R_P} = \frac{S}{V}, \tag{2}$$

where R_p is the pore radius (μm) and F_S is the pore shape factor (dimensionless). The value of F_S is closely related to the pore shape. For spherical pores, $F_S = 3$, while for columnar holes

$$F_S = 2 + \frac{1}{\beta}, \tag{3}$$

where β is the height-diameter ratio, and $\beta > 1$. Moreover, the discussion of the cylindrical pore shape factor is meaningless. The relationship between F_S and the height-diameter ratio is shown in Figure 5. The value of F_S is between 2 and 3. The higher the height-diameter ratio is, the closer F_S is to 2. For the pores inside the rock, the height-diameter ratio is not very high, and the shape is close to an ellipsoid. Therefore, F_S is set to 2.4 in this paper.

According to equations (1) to (3), the following can be obtained:

$$R_P = 0.012 T_2. \tag{4}$$

According to equation (4), the T2 spectrum curve can be transformed into the pore size distribution curve. To determine which pore types contribute to the reduction in porosity in the red sandstone, it is necessary to study the classification of pores.

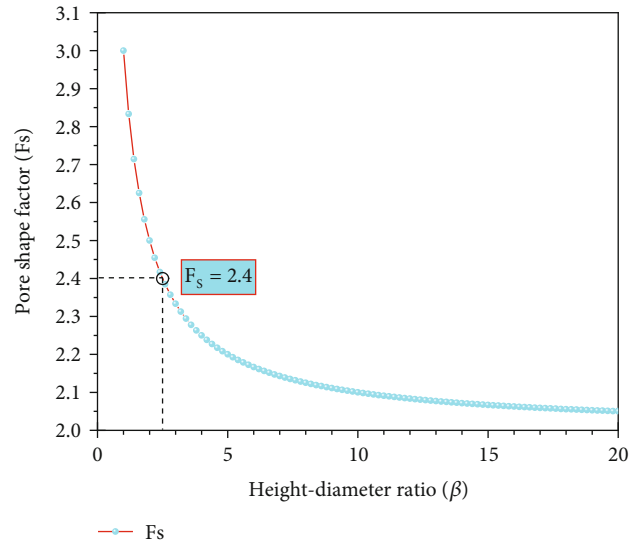

Figure 5: Change in the pore shape factor with the height-diameter ratio (when $\beta < 2$, F_S is relatively discrete, and when $\beta > 4$, F_S is relatively continuous).

At present, researchers have not established a unified standard for the classification of the pore size and have proposed different classification methods. Among them, Xiao [47] divided pores into two types: large pores ($R_p \geq 50\,\mu m$) and small pores ($R_p < 50\,\mu m$). Yang [48] partitioned pores into small pores ($R_p < 0.1\,\mu m$), medium pores ($0.1\,\mu m < R_p < 1\,\mu m$) and large pores ($R_p \geq 1\,\mu m$). Li [7] divided pores into micropores ($R_p < 0.1\,\mu m$), small pores ($0.1\,\mu m \leq R_p < 1\,\mu m$), medium pores ($1\,\mu m \leq R_p < 10\,\mu m$), and large pores ($R_p \geq 10\,\mu m$). In this paper, the red sandstone pore size is divided into four types, namely, micropores ($0 < R_p < 25$ nm), minipores (25 nm $< R_p < 50$ nm), mesopores (50 nm $< R_p < 1000$ nm), and macropores ($R_p > 1\,\mu m$) with reference to equation (4) and previous classification methods, as shown in Figure 6.

As shown in Figure 6, the pores in the red sandstone are mainly micro- and mesopores, and the content of these two types of pores accounts for approximately 85% of the total porosity. There is no obvious change in the content of micro- and minipores with the freeze-thaw weathering cycles. In addition, the content of meso- and macropores first decreased and then increased with increasing freeze-thaw weathering cycles, revealing a consistency with the change in the red sandstone porosity. Figure 6 shows that after 20 freeze-thaw weathering cycles, the content of mesopores is greatly reduced, and the porosity is reduced by 0.84%, accounting for 25.73% of the content of mesopores. Over 20-60 freeze-thaw weathering cycles, the content of mesopores continued to decrease, and the rate of decrease had relatively decelerated, reaching a minimum after 60 freeze-thaw weathering cycles. Subsequently, as the number of freeze-thaw weathering cycles continued to increase, the content

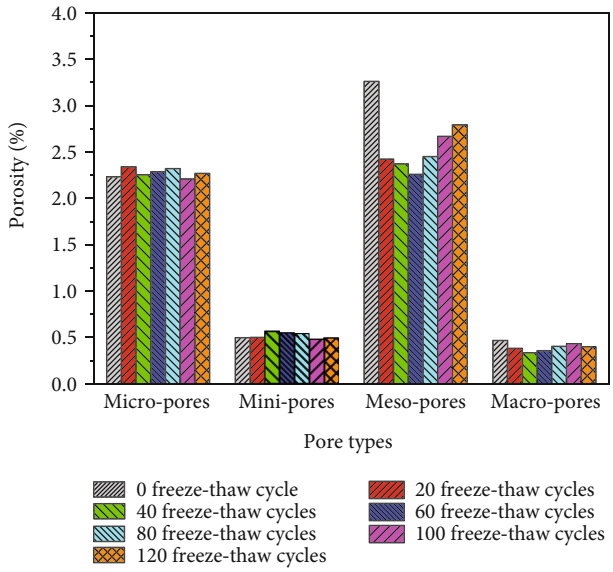

Figure 6: Change in the pore content of the four types with the freeze-thaw weathering cycles.

of mesopores gradually increased, and the growth rate remained relatively stable. The evolution trend of the macropore content is basically the same as that of the mesopores, but the change range is not large. Therefore, it could be inferred that the change in the porosity of the red sandstone is mainly due to the change in the pore content of meso- and macropores, among which the mesopores play a major role.

3.4. Pore Connectivity. Under the effect of pore fluid surface tension, the water in small pores does not flow, while in large pores, it flows freely. In the NMR test, the pore radius is proportional to the T2 value. Therefore, there is a T2 value that divides the pore fluid into bound fluid and free fluid, which is called the $T2_{cutoff}$ value [31].

The $T2_{cutoff}$ value divides the rock sample porosity into the bound fluid index (BVI) and free fluid index (FFI) by dividing the T2 spectrum distribution. Therefore, the determination of the $T2_{cutoff}$ value is particularly important for pore division purposes. In this paper, centrifuge technology is applied to determine the $T2_{cutoff}$ value, i.e., the samples are subjected to NMR testing at 100% saturation and bound-water saturation.

As shown in Figure 7, for the same rock samples, a horizontal line is plotted from the centrifugal porosity accumulation curve to the 100% saturated porosity accumulation curve, and a vertical line is then drawn from the intersection point to the T2 axis. The T2 value at the intersection point is the $T2_{cutoff}$ value.

According to the method shown in Figure 7, the $T2_{cutoff}$ value of the samples over every 20 freeze-thaw weathering cycles was obtained, and the irreducible fluid porosity (IFP), movable fluid porosity (MFP), BVI, FFI and other parameters of the samples were calculated, as summarized in Table 2.

Moreover, the permeability represents the fluid transferability of porous media, which is an intuitive representation of the pore connectivity. Studies have shown that the Timur-Coates model exhibits a good universality in different rock core tests. The relationship between the permeability and T2 value is expressed as equation (5):

$$K = \left(\frac{\Phi}{C}\right)^{m} \times \left(\frac{\mathrm{FFI}}{\mathrm{BVI}}\right)^{n}, \tag{5}$$

where K is the permeability, Φ is the porosity, and m, n, and C are Timur-Coates model parameters. Scholars have performed many experiments to determine the values of these model parameters. Based on previous studies, this paper assigns empirical values of 4, 2, and 10 to m, n, and C, respectively [31]. To directly reflect the characteristics of the pore connectivity with the freeze-thaw weathering cycles, the changes in porosity, IFP, MFP, $T2_{cutoff}$ value, and permeability are plotted in Figures 8 and 9.

As shown in Figure 8, after 120 freeze-thaw weathering cycles, the $T2_{cutoff}$ value of the red sandstone decreased from 4.4 to 2.13 ms, indicating that there were factors that impacted the pore size and pore connectivity, thus reducing the $T2_{cutoff}$ value by 51.59%. However, it is difficult to reflect the evolution of the red sandstone pore structure from the change in the $T2_{cutoff}$ value. Fortunately, IFP and MFP obtained by the $T2_{cutoff}$ value could more clearly reflect the change in the pore structure.

The changes in porosity, IFP, and MFP with the freeze-thaw weathering cycles are shown in Figure 8. It can be clearly seen that there exists a strong correlation between Δporosity and ΔMFP, which shows that the change in the red sandstone porosity is primarily caused by the change in the movable fluid porosity. Before 60 freeze-thaw weathering cycles, the amount of change in MFP was slightly larger than that in the porosity, and the amplitude of change tended to remain consistent. After 60 freeze-thaw weathering cycles, the amount of change in MFP gradually decreased. This occurred due to the decrease in the $T2_{cutoff}$ value, which represents the increase in the pore size range of MFP.

The changes in Δporosity, ΔMFP, and $T2_{cutoff}$ value indicate that the pore size changed during the freeze-thaw weathering process. The permeability is largely determined by the pore throat size, which is closely related to the pore size, so the permeability is a better indicator of the pore connectivity. As shown in Figure 9, after 20 freeze-thaw weathering cycles, the permeability suddenly decreased by 68.93%, from 0.285 to 0.089 mD. Combined with the previous analysis of the porosity, this may be due to the larger pores becoming partially blocked, reducing the pore throat size and porosity. During the process from 60 to 120 freeze-thaw weathering cycles, the permeability increased by 211.54%. This occurs due to the clogging effect gradually decreasing, and at the same time, under the effect of frost heave, the pore throat size and pore size gradually increasing.

3.5. Water-Rock Interactions. The samples are recovered from the frozen state to the thawed state through the water phase in this experiment. When water enters the pores and

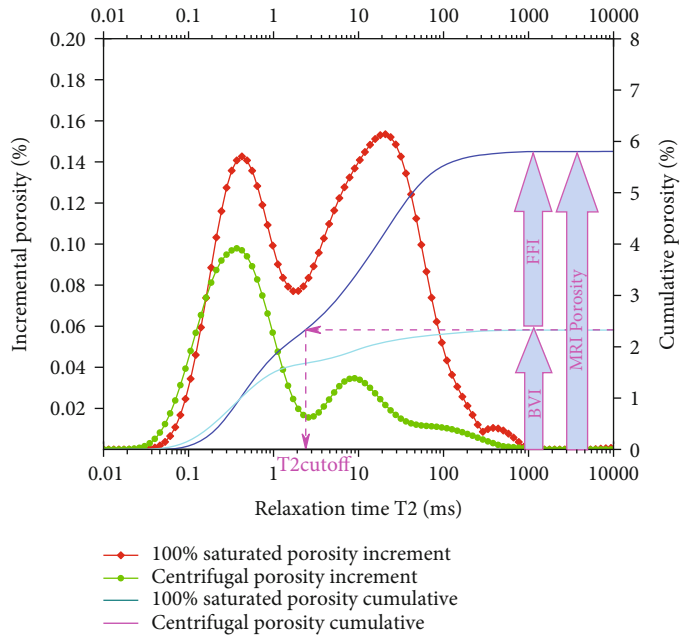

Figure 7: Schematic diagram of the $T2_{cutoff}$ value determination method.

Table 2: Average pore connectivity parameters calculated.

Freeze-thaw cycles	0	20	40	60	80	100	120
Porosity (%)	6.516	5.660	5.482	5.475	5.688	5.695	5.803
IFP (%)	2.681	2.845	2.841	2.706	2.623	2.364	2.313
MFP (%)	3.835	2.815	2.641	2.769	3.065	3.331	3.490
BVI (%)	41.147	50.269	51.827	49.432	46.116	41.503	39.859
FFI (%)	58.853	49.731	48.173	50.568	53.884	58.497	60.141
$T2_{cutoff}$	4.4	4.2	3.74	3.2	2.77	2.4	2.13

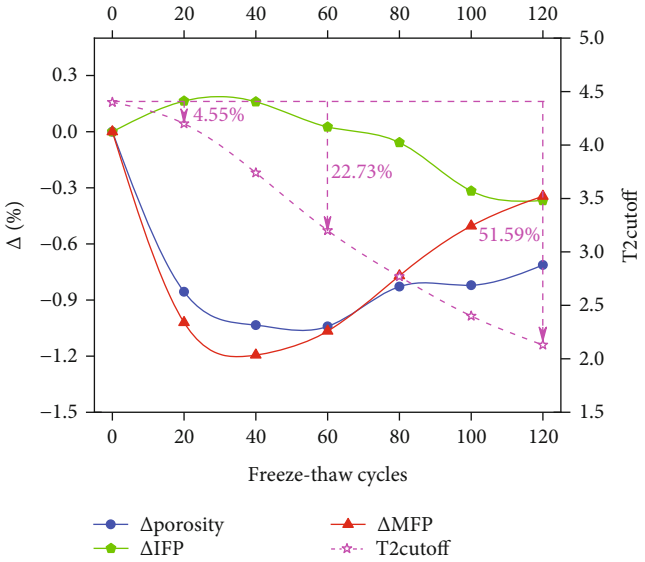

Figure 8: The change in the pore connectivity parameters with the freeze-thaw weathering cycles (top and right axes associated with $T2_{cutoff}$).

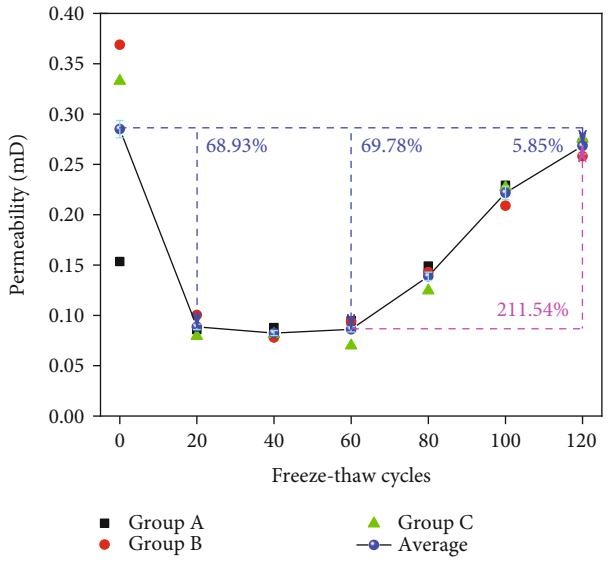

Figure 9: The change in the permeability with the freeze-thaw weathering cycles.

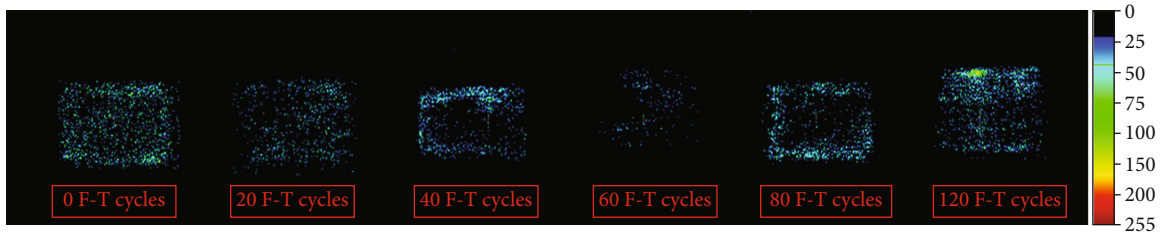

(a) Images of the upper slice

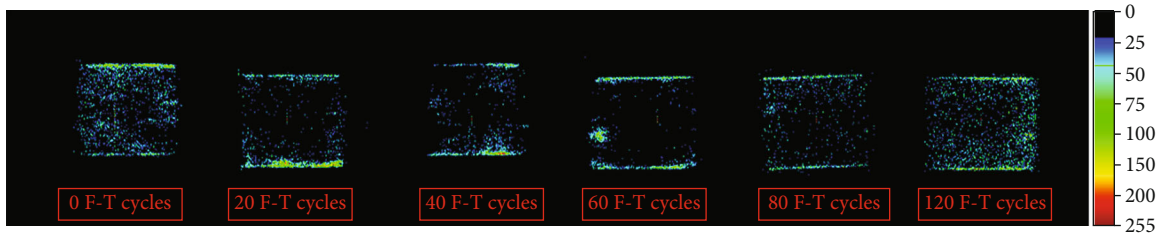

(b) Images of the middle slice

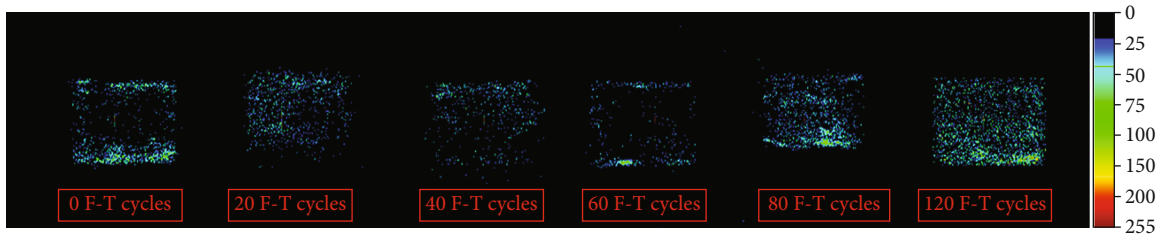

(c) Images of the lower slice

Figure 10: MRI images of the red sandstone during the freeze-thaw weathering process.

cracks in the samples, water-rock interactions (including hydrophysical and hydrochemical effects) will change the rock physical and mechanical properties [41]. Hydrophysical effects alter the rock physical and mechanical properties by changing the interconnection between mineral particles and their physical occurrence through their water absorption and water solubility. Hydrochemical effects alter the mineral composition and microstructure through chemical corrosion, thus changing the rock physical and mechanical properties, such as the particle size, mineral properties, and crack morphology. Hydrochemical effects are more pronounced in acidic and alkaline solutions but less likely in neutral solutions. This experiment was performed with distilled water. Therefore, water-rock interactions mainly affect the microscopic characteristics of the rock through hydrochemical effects.

XRD analysis of this kind of red sandstone shows that the mineral composition mainly includes quartz, feldspar, chlorite, calcite, and clay minerals. Among them, montmorillonite among the clay minerals belongs to the strongly hydrophilic clay minerals, whose volume increases by more than 600% after water absorption. The water-rock interaction reaction is shown in equation (6).

$$(\mathrm{Na, Ca})_{0.33}(\mathrm{Al, Mg})_2(\mathrm{Si_4O_{10}})(\mathrm{OH})_2 + n\mathrm{H_2O} \longrightarrow (\mathrm{Na, Ca})_{0.33}(\mathrm{Al, Mg})_2(\mathrm{Si_4O_{10}})(\mathrm{OH})_2 \bullet n\mathrm{H_2O}. \quad (6)$$

Rock is a porous medium. In the freeze-thaw process, liquid water penetrates the rock along the microgaps between the interfaces of particles and the microcracks in the rock. The montmorillonite near rock fractures and pores absorbs water, and the expanded volume occupies part of the pore space. Therefore, the porosity detected by NMR decreases. According to the pore size classification results, the expanded volume of montmorillonite mostly occupies the pore space of the mesopores, and this hydrophysical effect largely occurs in the first 20 freeze-thaw weathering cycles.

3.6. Magnetic Resonance Imaging (MRI). The MRI module of the NMR testing system detects the hydrogen atom distribution of water in saturated rock samples and projects the detection information of a certain layer thickness on a horizontal plane to reflect the pore information of the rock in the form of two-dimensional images.

The rock sample is divided into three slices or detection layers, i.e., upper, middle, and lower layers, with a slice thickness of 10 mm and a slice spacing of 5 mm. Coronal imaging is applied, and the imaging results are shown in Figure 10. The black part of Figure 10 represents the absence of pores or the sample matrix. The projection of all the pores in the detection layer on the same horizontal plane forms bright or dark spots in the images, which represent the pore size and pore distribution. As shown in the legend, the closer the spot colour is to blue, the lower the degree of pore superposition in the slice detection space is, and the smaller the

spot is, the smaller the pore size is. Correspondingly, the larger the corresponding parameter of the spot colour is, the denser the pore distribution is in the slice detection space, and the larger the spot is, the larger the pore size is.

According to the MRI images shown in Figure 10, in the initial state, the internal pore distribution of the red sandstone is scattered, with both small and large pores, which is consistent with the results of the T2 spectrum distribution, indicating that the experimental data are reasonable.

After 0-20 freeze-thaw weathering cycles, the green spots in the MRI images were greatly reduced, and there were more dark blue small spots, indicating that the original larger pores of this sandstone suddenly decreased. This likely occurred because the montmorillonite in the pores expanded with water absorption, and the original larger pores provided space for the expanded volume.

After 20-60 freeze-thaw weathering cycles, the number of green and blue spots in the MRI images decreased slightly, and the number of blue spots slightly increased, but the overall change was not notable, indicating that during this process, micropore initiation occurred, and a small number of the large pores shrank.

After 60-120 freeze-thaw weathering cycles, the spots in the images gradually brightened, which occurred because the water absorption process of montmorillonite reached saturation, and the effect of the frost heaving force continuously developed, thereby connecting and expanding the pores, which was also the main reason for the increased porosity in this process.

After 60 freeze-thaw cycles, the spots in the images gradually brightened, which occurred because the water absorption process of montmorillonite reached saturation, the effect of the frost heaving force continuously developed, connected and expanded the pores, and the pore size gradually increased, which was also the main reason for the increased porosity in this process. After the completion of 120 freeze-thaw weathering cycles, debris was found in the freeze-thaw device, which was the result of montmorillonite falling off after absorbing water during the process, thus accelerating the deterioration of the rock physical and mechanical properties.

4. Conclusions

In this study, the porosity, T2 spectrum, and MRI in the freeze-thaw weathering cycles of red sandstone were obtained by NMR technology. The evolution rules of pore size, pore type, permeability, and pore connectivity were analyzed. The experimental phenomena were discussed, and the following conclusions were obtained:

(1) The porosity evolution of this red sandstone can be divided into three stages, namely, the abrupt decrease in porosity over 0-20 freeze-thaw weathering cycles, the slow decrease in porosity over 20-60 freeze-thaw weathering cycles, and the steady increase in porosity over 60-120 freeze-thaw weathering cycles, which does not always increase nonlinearly.

(2) The changes in the T2 spectrum distribution, pore size, MRI images, and permeability were positively correlated with the porosity during the freeze-thaw weathering process. Furthermore, the change in the porosity of the red sandstone was basically consistent with that of MFP, and the abrupt decrease in the porosity mainly originated from the decrease in the mesopores ranging from 50 to 100 nm

(3) The evolution of the pore structure of this red sandstone is the result of the hydrophysical effects caused by water absorption expansion of montmorillonite and the frost heaving caused by the water-ice phase transition, and these two effects are mutually exclusive. The influence of the above hydrophysical effects only occurred in the early stage of the experiment, and the frost heaving effects dominated the evolution of the pore structure during the continuous freeze-thaw weathering cycles in the late stage

The research results of this paper have a certain reference value to better understand the pore structure evolution of red sandstone in cold regions and its physical and mechanical properties across various scales and have a certain guiding significance for sandstone engineering in cold regions. It should be pointed out that the pore structure evolution of red sandstone is influenced by many factors, such as the temperature, confining pressure, chemical environment, and multiscale coupling effect, which deserve a more in-depth study.

Data Availability

Most of the data supporting this study are included in this article and all of the data are available from the corresponding author on reasonable request.

Conflicts of Interest

The authors declare that they have no conflicts of interest.

Acknowledgments

This research was jointly supported by the National Natural Science Foundation of China (51774323), Hunan Province Natural Science Foundation of China (2020JJ4704 and 2020JJ4712), and the Fundamental Research Funds for the Central Universities of Central South University, China (2020zzts700). The authors would like to thank the School of Resources and Safety Engineering and the Research Center for Mining Engineering and Technology in Cold Regions of Central South University for the support of the experimental devices, and at the same time, thank the scholars who put forward valuable suggestions in the process of writing and revising this paper.

References

[1] M. Deprez, T. de Kock, G. de Schutter, and V. Cnudde, "A review on freeze-thaw action and weathering of rocks," *Earth-Science Reviews*, vol. 203, article 103143, 2020.

[2] J. Chen, J. Zhao, S. Zhang, Y. Zhang, F. Yang, and M. Li, "An experimental and analytical research on the evolution of mining cracks in deep floor rock mass," *Pure and Applied Geophysics*, 2020.

[3] J. Wang, Y. Zhang, Z. Qin, S. Song, and P. Lin, "Analysis method of water inrush for tunnels with damaged water-resisting rock mass based on finite element method-smooth particle hydrodynamics coupling," *Computers and Geotechnics*, vol. 126, article 103725, 2020.

[4] C. Xia, Z. Lv, Q. Li, J. Huang, and X. Bai, "Transversely isotropic frost heave of saturated rock under unidirectional freezing condition and induced frost heaving force in cold region tunnels," *Cold Regions Science and Technology*, vol. 152, pp. 48–58, 2018.

[5] H. Lin, D. Lei, R. Yong, C. Jiang, and S. Du, "Analytical and numerical analysis for frost heaving stress distribution within rock joints under freezing and thawing cycles," *Environmental Earth Sciences*, vol. 79, no. 12, article 30512, 2020.

[6] H. Lin, R. Cao, X. Fan, and Y. Wang, "Damage and fracture behavior of rock," *Advances in Civil Engineering*, vol. 2019, Article ID 8476537, 3 pages, 2019.

[7] J. Li, R. B. Kaunda, and K. Zhou, "Experimental investigations on the effects of ambient freeze-thaw cycling on dynamic properties and rock pore structure deterioration of sandstone," *Cold Regions Science and Technology*, vol. 154, pp. 133–141, 2018.

[8] K. Abdolghanizadeh, M. Hosseini, and M. Saghafiyazdi, "Effect of freezing temperature and number of freeze-thaw cycles on mode I and mode II fracture toughness of sandstone," *Theoretical and Applied Fracture Mechanics*, vol. 105, article 102428, 2020.

[9] T. De Kock, M. A. Boone, T. De Schryver et al., "A pore-scale study of fracture dynamics in rock using x-ray micro-CT under ambient freeze-thaw cycling," *Environmental Science & Technology*, vol. 49, no. 5, pp. 2867–2874, 2015.

[10] J. Xu, A. Haque, W. Gong et al., "Experimental study on the bearing mechanisms of rock-socketed piles in soft rock based on micro X-ray CT analysis," *Rock Mechanics and Rock Engineering*, vol. 53, no. 8, pp. 3395–3416, 2020.

[11] L. Chen, X. Mao, S. Yang, C. An, and P. Wu, "Experimental investigation on dynamic fracture mechanism and energy evolution of saturated yellow sandstone under different freeze-thaw temperatures," *Advances in Civil Engineering*, vol. 2019, Article ID 2375276, 16 pages, 2019.

[12] J. Li, R. B. Kaunda, L. Zhu, K. Zhou, and F. Gao, "Experimental study of the pore structure deterioration of sandstones under freeze-thaw cycles and chemical erosion," *Advances in Civil Engineering*, vol. 2019, Article ID 9687843, 12 pages, 2019.

[13] B. Ke, K. Zhou, H. Deng, and F. Bin, "NMR pore structure and dynamic characteristics of sandstone caused by ambient freeze-thaw action," *Shock and Vibration*, vol. 2017, 10 pages, 2017.

[14] J. Zhang, H. Deng, J. Deng, and H. Guo, "Influence of freeze-thaw cycles on the degradation of sandstone after loading and unloading," *Bulletin of Engineering Geology and the Environment*, vol. 79, no. 4, pp. 1967–1977, 2020.

[15] J. B. Murton, O. Kuras, M. Krautblatter et al., "Monitoring rock freezing and thawing by novel geoelectrical and acoustic techniques," *Journal of Geophysical Research: Earth Surface*, vol. 121, no. 12, pp. 2309–2332, 2016.

[16] Y. Liu, Y. Cai, S. Huang, Y. Guo, and G. Liu, "Effect of water saturation on uniaxial compressive strength and damage degree of clay-bearing sandstone under freeze-thaw," *Bulletin of Engineering Geology and the Environment*, vol. 79, no. 4, pp. 2021–2036, 2020.

[17] C. Liu, H. Deng, X. Chen, D. Xiao, and B. Li, "Impact of rock samples size on the microstructural changes induced by freeze–thaw cycles," *Rock Mechanics and Rock Engineering*, vol. 53, 2020.

[18] C. Liu, H. Deng, H. Zhao, and J. Zhang, "Effects of freeze-thaw treatment on the dynamic tensile strength of granite using the Brazilian test," *Cold Regions Science and Technology*, vol. 155, pp. 327–332, 2018.

[19] J. Hu, Q. Ren, S. Ma et al., "Macroscopic and microscopic trans-scale characteristics of pore structure of mine grouting materials," *Transactions of Nonferrous Metals Society of China*, vol. 29, no. 5, pp. 1067–1081, 2019.

[20] J. Hu, Q. Ren, X. Ding, and Q. Jiang, "Trans-scale relationship analysis between the pore structure and macro parameters of backfill and slurry," *Royal Society Open Science*, vol. 6, no. 6, article 1903896, 2019.

[21] C. Zhai, S. Wu, S. Liu, L. Qin, and J. Xu, "Experimental study on coal pore structure deterioration under freeze–thaw cycles," *Environmental Earth Sciences*, vol. 76, no. 15, 2017.

[22] H. Jia, S. Ding, Y. Wang, F. Zi, Q. Sun, and G. Yang, "An NMR-based investigation of pore water freezing process in sandstone," *Cold Regions Science and Technology*, vol. 168, article 102893, 2019.

[23] C. Lyu, Z. Ning, Q. Wang, and M. Chen, "Application of NMR t2 to pore size distribution and movable fluid distribution in tight sandstones," *Energy & Fuels*, vol. 32, no. 2, pp. 1395–1405, 2018.

[24] F. Wang, P. Cao, Y. Wang, R. Hao, J. Meng, and J. Shang, "Combined effects of cyclic load and temperature fluctuation on the mechanical behavior of porous sandstones," *Engineering Geology*, vol. 266, article 105466, 2020.

[25] K. Park, B. Y. Lee, K. Lee, and D. Kim, "Analysis of effects of rock physical properties changes from freeze-thaw weathering in Ny-Ålesund region: part 2-correlations and prediction of weathered properties," *Applied Sciences*, vol. 10, no. 10, article 3392, 2020.

[26] C. Zhu, M. He, M. Karakus, X. Cui, and Z. Tao, "Investigating toppling failure mechanism of anti-dip layered slope due to excavation by physical modelling," *Rock Mechanics and Rock Engineering*, 2020.

[27] C. Zhu, Z. Tao, S. Yang, and S. Zhao, "V shaped gully method for controlling rockfall on high-steep slopes in China," *Bulletin of Engineering Geology and the Environment*, vol. 78, no. 4, pp. 2731–2747, 2019.

[28] X. Wang, C. Liu, S. Chen, L. Chen, K. Li, and N. Liu, "Impact of coal sector's de-capacity policy on coal price," *Applied Energy*, vol. 265, article 114802, 2020.

[29] L. Liu, G. Qin, S. Qin, and G. Tao, "Simulation of the volumetric deformation and changes in the pore structure of unsaturated cement-based materials subjected to freezing/thawing," *Construction and Building Materials*, vol. 230, article 116964, 2020.

[30] Z. Jiang, S. Yu, H. Deng, J. Deng, and K. Zhou, "Investigation on microstructure and damage of sandstone under cyclic dynamic impact," *IEEE Access*, vol. 7, pp. 133145–133158, 2019.

[31] Z. Jiang, H. Deng, T. Liu, G. Tian, and L. Tang, "Study on microstructural evolution of marble under cyclic dynamic impact based on NMR," *IEEE Access*, vol. 7, pp. 138043–138055, 2019.

[32] L. Weng, Z. Wu, A. Taheri, Q. Liu, and H. Lu, "Deterioration of dynamic mechanical properties of granite due to freeze-thaw weathering: Considering the effects of moisture conditions," *Cold Regions Science and Technology*, vol. 176, article 103092, 2020.

[33] L. Martins, G. Vasconcelos, P. B. Lourenço, and C. Palha, "Influence of the freeze-thaw cycles on the physical and mechanical properties of granites," *Journal of Materials in Civil Engineering*, vol. 28, no. 5, article 04015201, 2016.

[34] S. Huang, Q. Liu, A. Cheng, Y. Liu, and G. Liu, "A fully coupled thermo-hydro-mechanical model including the determination of coupling parameters for freezing rock," *International Journal of Rock Mechanics and Mining Sciences*, vol. 103, pp. 205–214, 2018.

[35] B. Chen, S. Zhang, Y. Li, Z. Li, and H. Zhou, "Physical simulation study of crack propagation and instability information discrimination of rock-like materials with faults," *Arabian Journal of Geosciences*, vol. 13, no. 18, article 96618, 2020.

[36] C.-Y. Hou, Z.-D. Cui, and L. Yuan, "Accumulated deformation and microstructure of deep silty clay subjected to two freezing-thawing cycles under cyclic loading," *Arabian Journal of Geosciences*, vol. 13, no. 12, article 45212, 2020.

[37] D. Liu, Z. Gu, R. Liang et al., "Impacts of pore-throat system on fractal characterization of tight sandstones," *Geofluids*, vol. 2020, Article ID 4941501, 17 pages, 2020.

[38] I. N. Grubeša, M. Vračević, J. Ranogajec, and S. Vučetić, "Influence of pore-size distribution on the resistance of clay brick to freeze-thaw cycles," *Materials*, vol. 13, no. 10, article 236410, p. 2364, 2020.

[39] X. Cai, Z. Zhou, K. Liu, X. Du, and H. Zang, "Water-weakening effects on the mechanical behavior of different rock types: phenomena and mechanisms," *Applied Sciences*, vol. 9, no. 20, article 445020, p. 4450, 2019.

[40] W. Yan, J. Sun, N. Golsanami et al., "Evaluation of wettabilities and pores in tight oil reservoirs by a new experimental design," *Fuel*, vol. 252, pp. 272–280, 2019.

[41] Y. Lin, K. Zhou, R. Gao, J. Li, and J. Zhang, "Influence of chemical corrosion on pore structure and mechanical properties of sandstone," *Geofluids*, vol. 2019, Article ID 7320536, 15 pages, 2019.

[42] B. Liu, Y. Ma, N. Liu, Y. Han, D. Li, and H. Deng, "Investigation of pore structure changes in Mesozoic water-rich sandstone induced by freeze-thaw process under different confining pressures using digital rock technology," *Cold Regions Science and Technology*, vol. 161, pp. 137–149, 2019.

[43] C. Naber, F. Kleiner, F. Becker et al., "C-S-H pore size characterization via a combined nuclear magnetic resonance (NMR)-Scanning electron microscopy (SEM) surface relaxivity calibration," *Materials*, vol. 13, no. 7, article 17797, 2020.

[44] L. Yan, L. Liu, S. Zhang, D. Lan, and J. Liu, "Testing of weakly weathered granites of different porosities using a split hopkinson pressure bar technique," *Advances in Civil Engineering*, vol. 2018, Article ID 5267610, 11 pages, 2018.

[45] M. Saidian and M. Prasad, "Effect of mineralogy on nuclear magnetic resonance surface relaxivity: a case study of Middle Bakken and Three Forks formations," *Fuel*, vol. 161, pp. 197–206, 2015.

[46] M. Y. Shumskayte and V. N. Glinskikh, "Relation of NMR parameters with specific surface and resistivity of shaly sandstone and siltstone samples: experimental study," *Russian Geology and Geophysics*, vol. 57, no. 10, pp. 1509–1514, 2016.

[47] Y. Zhang, L. Xiao, G. Liao, and Y.-Q. Song, "Direct correlation of diffusion and pore size distributions with low field NMR," *Journal of Magnetic Resonance*, vol. 269, pp. 196–202, 2016.

[48] N. Yang, K. Zhou, T. Lei, J. Li, and F. Bin, "Sandstones dynamic mechanical properties and failure characteristics under freeze-thaw cycles," *Transactions of Nonferrous Metals Society of China*, vol. 26, no. 10, pp. 2181–2187, 2016.